Protist, Vol. 171, 125717, xx 2020
http://www.elsevier.de/protis
Published online date 7 February 2020

Protist

ORIGINAL PAPER

Unique Dynamics of Paramylon Storage in the Marine Euglenozoan *Diplonema papillatum*

Ingrid Škodová-Sveráková[a,b], Galina Prokopchuk[a], Priscila Peña-Diaz[a,c], Kristína Záhonová[a,c], Martin Moos[d], Anton Horváth[b], Petr Šimek[d], and Julius Lukeš[a,e,1]

[a]Institute of Parasitology, Biology Centre, Czech Academy of Sciences, České Budějovice (Budweis), Czech Republic
[b]Faculty of Natural Sciences, Comenius University, Bratislava, Slovakia
[c]Faculty of Science, Charles University, BIOCEV, Vestec, Czech Republic
[d]Institute of Entomology, Biology Centre, Czech Academy of Sciences, České Budějovice (Budweis), Czech Republic
[e]Faculty of Sciences, University of South Bohemia, České Budějovice (Budweis), Czech Republic

Submitted September 10, 2019; Accepted February 2, 2020
Monitoring Editor: Michael Ginger

Diplonemids belong to the most diverse and abundant marine protists, which places them among the key players of the oceanic ecosystem. Under in vitro conditions, their best-known representative *Diplonema papillatum* accumulates in its cytoplasm a crystalline polymer. When grown under the nutrient-poor conditions, but not nutrient-rich conditions, *D. papillatum* synthesizes a β-1,3-glucan polymer, also known as paramylon. This phenomenon is unexpected, as it is in striking contrast to the accumulation of paramylon in euglenids, since these related flagellates synthesize this polymer solely under nutrient-rich conditions. The capacity of *D. papillatum* to store an energy source in the form of polysaccharides when the environment is poor in nutrients is unexpected and may contribute to the wide distribution of these protists in the ocean.

Key words: β-1,3-glucan; paramylon; trehalose; diplonemids; paramylon synthase.

Introduction

Protists represent the bulk of extant eukaryotic diversity, yet their abundance and ecological significance in the oceans is being appreciated only recently (de Vargas et al. 2015; Worden et al. 2015). The capacity of protists to inhabit virtually every niche in the world ocean is reflected in their metabolism, which is often highly complex and versatile due to their gene-rich genomes (Keeling et al. 2014; Keeling and del Campo 2017).

One of the prominent groups are diplonemids, a sister clade of the mostly parasitic kinetoplastids and the free-living euglenids, all belonging to the phylum Euglenozoa (Adl et al. 2018). Diplonemids are the most diverse and the 6th most species-rich

[1]Corresponding author;
e-mail jula@paru.cas.cz (J. Lukeš).

https://doi.org/10.1016/j.protis.2020.125717

group of marine protists (de Vargas et al. 2015; Flegontova et al. 2016). The available sequence data shows that they are non-photosynthetic, which is consistent with their preference for mesopelagic and bathypelagic habitats (Flegontova et al. 2016; Lara et al. 2009). So far, the only diplonemid experimentally studied to some extent is *Diplonema papillatum*, best-known for the unprecedented complexity of its mitochondrial genome and transcriptome (Valach et al. 2017). Moreover, studies implementing genetic modifications in *D. papillatum* have begun to turn this flagellate into a genetically tractable organism (Kaur et al. 2018).

D. papillatum has also been the subject of the only metabolic study performed on diplonemids so far, which revealed that they compartmentalize five of the first seven enzymes of the gluconeogenic pathway into peroxisomes, which are thus reminiscent of glycosomes (Morales et al. 2016). While hexokinase and phosphofructokinase do not seem to be expressed, *D. papillatum* was shown to perform gluconeogenesis. Consequently, it has been hypothesized that this protist is incapable of performing glycolysis, with the gluconeogenic flux originating from the metabolism of amino acids being routed through the pentose phosphate pathway (Morales et al. 2016). In trypanosomes and related flagellates, the first seven of 10 glycolytic enzymes are also compartmentalized in glycosomes, a hallmark of these protists (Bringaud et al. 2006; Opperdoes and Borst 1977). They metabolize glucose and amino acids, with proline and threonine being essential for energy production (Coustou et al. 2003; Millerioux et al. 2013). Gluconeogenesis has been reported from trypanosomes as a flux that may be directed through the pentose phosphate pathway for the regeneration of cytosolic NADPH (Allmann et al. 2013). This unique compartmentalization of glycolytic enzymes has been proposed as an adaptation to their specialized lifestyles (Haanstra et al. 2016; Szöor et al. 2014).

Although trypanosomes lack the capability of storing carbohydrates (Bakker et al. 2000), they may store carbon sources in the form of lipid droplets (Allmann et al. 2014; Smith et al. 2017). Moreover, members of the genus *Leishmania* differ from trypanosomes in that they synthesize a carbohydrate polymer that resembles a mannose polymer or mannan (Blum 1993). *Leishmania mexicana* was subsequently shown to synthesize and store β-1,2-mannan, a polymer of mannose. However, glycopolymers in *Leishmania* species are linked to the assembly of the glycocalyx coat and have an essential function in their infectivity and survival in the mammalian host (Ralton et al. 2003; Sernee et al. 2006). Thus, the polymer synthesis and remodeling mostly depend on the parasite life stage, rather than on carbon availability.

Out of the diverse euglenozoans with lifestyles ranging from parasitism to photosynthesis (Adl et al. 2018), only the euglenophytes carrying the secondary plastid are known to deposit glucose *via* β-1,3-glycosidic linkage, forming a storage polysaccharide known as paramylon (Kiss and Triemer 1988). However, outside of the euglenozoans, linear β-1,3-glucans are widely distributed in bacteria, haptophytes, fungi, lichens and some plants, where the polymer carries different names, such as curdlan, pachyman, laricinan or callose (Archibald et al. 1963; Aspinall and Kessler 1957; Clarke and Stone 1960; Harada et al. 1968; Warsi and Whelan 1957). Paramylon is an insoluble, linear β-1,3-glucan of high molecular mass, which occurs naturally in the crystalline form (Booy et al. 1981). Euglenids accumulate paramylon in granules, which may be widely distributed in the cytoplasm, may form caps over the pyrenoids or be packed together (Monfils et al. 2011). The various types of paramylon were separated into six morphological categories, all present in the diverse euglenids (Monfils et al. 2011).

The formation of this polysaccharide follows a general pathway where a uridine diphosphate glucose (UDP-Glc) donates the glucose moiety that is subsequently linked to form the growing polysaccharide. Glucose for the UDP-Glc precursor originates from various sources and the formation of the sugar nucleotide depends on UTP:α-D-glucose uridylyltransferase or UDP-Glc pyrophosphorylase (Muchut et al. 2018). In euglenids, paramylon formation requires the activity of paramylon synthase (Bäumer et al. 2011; Marechal and Goldemberg 1964; Tanaka et al. 2017), which is a membrane-bound enzyme complex of approximately 670 kDa belonging to the eukaryotic family of glycosyltransferases 48 (GT48) (Bäumer et al. 2011). So far, two glucan synthase-like genes, called EgGSL1 and EgGSL2, were found in *Euglena gracilis*. They code for proteins of 304 and 258 kDa, with 15 and 19 transmembrane domains, respectively (Tanaka et al. 2017). The synthesis of paramylon, however, relies on the activity of EgGSL2, which forms a complex with 37 and 54 kDa UDP-binding proteins (Tanaka et al. 2017). The activity of paramylon synthase is associated with the membrane fraction that surrounds the paramylon granules (Bäumer et al. 2011). Degradation of β-1,3-glucan involves the action of endo- and exo-β-1,3-glucanases found in various glyco-

side hydrolase families (Henrissat 1991; Henrissat and Bairoch 1996; Henrissat and Davies 1997).

Paramylon has been extensively studied in *E. gracilis*, where its synthesis is usually triggered by growth under the nutrient-rich conditions (Calvayrac et al. 1981), represented by either photosynthetic carbon assimilation or heterotrophic growth on a suitable carbon source, such as sugars or organic acids (Briand and Calvayrac 1980). The dynamics of paramylon synthesis in *E. gracilis* is influenced by light, as the metabolite accumulated during the dark phase may be consumed for chlorophyll synthesis in the presence of light (Calvayrac et al. 1981; Dwyer and Smillie 1970; Schwartzbach et al. 1975). When *E. gracilis* is cultured under carbon starvation, the breakdown of paramylon is triggered by light, while this process is slower in cells grown in the dark (Dwyer and Smillie 1970). Paramylon hydrolysis may also be triggered by several factors other than metabolic requirements, such as osmotic stress or environmental adaptations (Takenaka et al. 1997).

Recent studies demonstrated the usefulness of dietary paramylon for therapeutic purposes, namely its activity against fatty liver disease and its antitumor activity in mice, where it significantly reduced colon cancer (Nakashima et al. 2019; Watanabe et al. 2013). It has also been tested as a dietary supplement in mouse models, as it reduces development of adipocyte differentiation in human cell tissues and enhances the immune system (Kondo et al. 1992; Nakashima et al. 2019; Okouchi et al. 2019; Sugimoto et al. 2018).

In this report, we isolated and analyzed a carbohydrate polymer bearing β-1,3-glucan linkages from *D. papillatum* grown under carbon-poor conditions. The isolated polymer has the same properties as paramylon from *E. gracilis*. We show that accumulation of this polymer depends on specific physiological conditions encountered by diplonemids during their life cycle and possibly contributes to their success in the least habitable zones of the world oceans.

Results

Cell Growth in Carbon-depleted Conditions

We assessed the viability of *D. papillatum* in two different media: (1) a carbon-rich medium, or standard growth medium, and (2) a carbon-poor medium, in which the concentration of tryptone is 100× lower than that present in the standard growth medium. Since tryptone is the main carbon source in this medium, and to a lower extent, of nitrogen, hereafter we refer to them as carbon-rich and carbon-poor media. Both media had 3.6% salinity and contained 1% (v/v) horse serum. Inoculation of the cells into the carbon-poor medium resulted in a significant growth retardation and a switch of the cells into what may be considered a permanent stationary phase (Fig. 1A), as compared to the carbon-rich culture condition, under which the cells grew exponentially for 11 days (264 hrs) (Fig. 1A). A significant accumulation of cytosolic vesicles occurred in cells grown in the carbon-poor medium (Fig. 1B). When viewed with a light microscope, diplonema cells appeared to have higher motility in the carbon-poor medium as compared to the carbon-rich one, with their morphology unaltered (Fig. 1B).

Characterization of Paramylon

The carbohydrate polymer isolated from approximately 8×10^6 and 4×10^7 *E. gracilis* and *D. papillatum* cells, respectively, were subjected to acid hydrolysis in order to obtain monomers. Following this treatment, the samples were submitted to thin layer chromatography (TLC) to assess their composition (Fig. 2A). The monosaccharide profiles of *D. papillatum* cultivated in the carbon-poor medium and *E. gracilis* cultivated in the complete medium, which was used as control, comprise of a single band co-migrating with the glucose standard (Fig. 2A). The total monosaccharide profiles of *D. papillatum* grown either in the carbon-rich or carbon-poor media (Fig. 2B) display more complexity and consisted of galactose, glucose, ribose, rhamnose and one monosaccharide that did not match any of the used standards (ribose, mannose, glucose, rhamnose, galactose, arabinose). The ratio between the determined monosaccharides strongly depended on the cultivation medium, as was shown by the TLC and gas chromatography–mass spectrometry (GC–MC) analyses of saccharides. Indeed, both methods revealed an increase in glucose and other sugars levels, except fructose and myo-inositol (Fig. 2B; Table 1). Accumulation of sugars was noticeably lower in cells grown in the carbon-rich medium (Fig. 2B).

Identification of β-1,3-glucan Linkage Within the Cells

To determine the presence of a polymer harbouring a β-1,3-glucan linkage within the cells, *D. papil-*

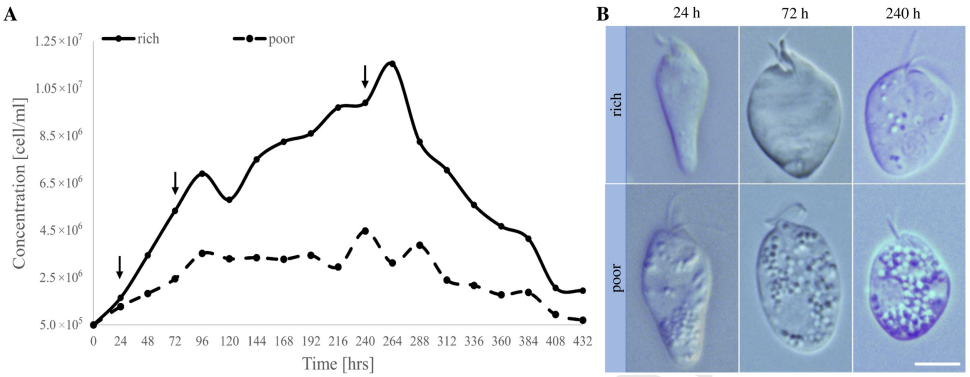

Figure 1. Growth (**A**) and morphology (**B**) of *D. papillatum* under different cultivation conditions. 5×10^5 cells were inoculated into the carbon-rich (full line) and carbon-poor media (dashed line). The dynamics of growth was monitored every 24 hours over 18 days, when the number of cells dropped to initial concentration. (B) Morphology of cells was examined by light microscopy at 24, 72 and 240 hours (see black arrows in A). Scale bar – 10 μm.

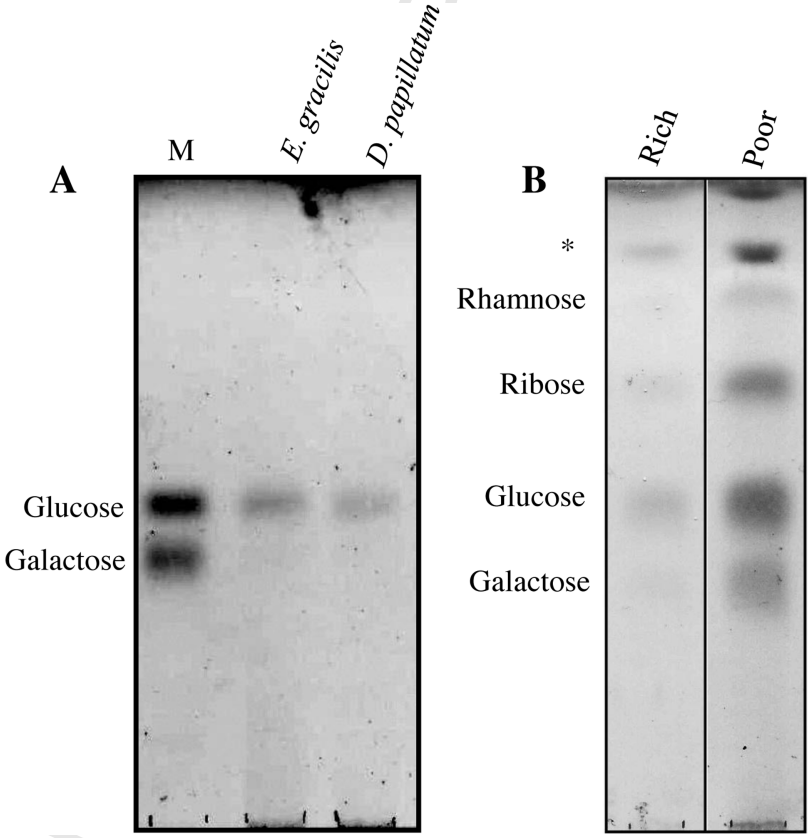

Figure 2. TLC analysis of monosaccharides. **(A)** Hydrolyzed β-1,3-polymers from *E. gracilis* and *D. papillatum.* **(B)** Total monosaccharide profile of *D. papillatum* grown in the carbon-rich (rich) and carbon-poor (poor) media. Individual monosaccharides were identified using standards resolved on TLC along with the samples. *, does not match to any of the available standards.

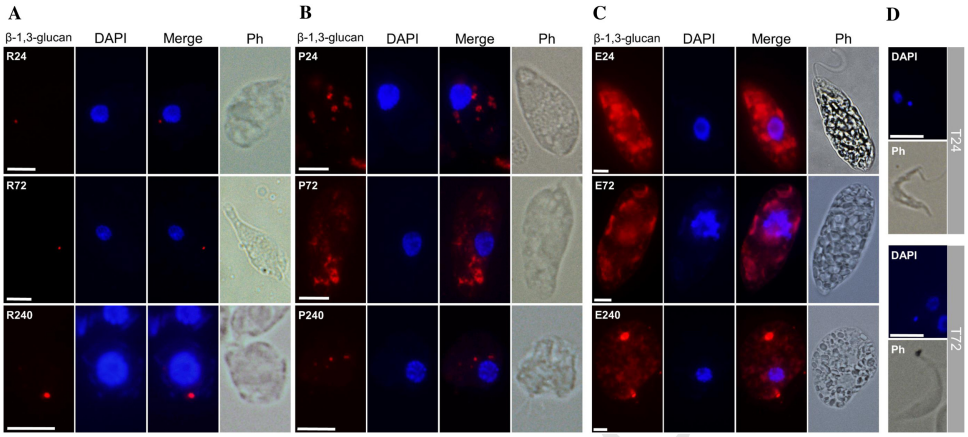

Figure 3. Detection of β-1,3-glucan by immunofluorescence, in *D. papillatum* grown in the carbon-rich (**A**) and carbon-poor conditions (**B**), *Euglena gracilis* (**C**) and *Trypanosoma brucei* (**D**). *E. gracilis* and *T. brucei* served as positive and negative controls, respectively. Cells were treated at 24 (R24, P24, E24 and T24), 72 (R72, P72, E72 and T72) and 240 hours (R240, P240 and E240) with anti-β-1,3-glucan monoclonal antibody and visualized using red-fluorescent Alexa Fluor 555 goat anti-mouse antibody. DAPI was used to stain the nucleus. Ph, phase contrast. Scale bar – 5 μm.

Table 1. GC-MS analysis of polyols and saccharides in *D. papillatum.*

Medium	Rich	Poor
	Concentration [nmol/6 × 10^6 cells]	
Ribose	0.022 ± 0.002	0.032 ± 0.007
Arabinitol	0.031 ± 0.004	0.100 ± 0.027
Ribitol	0.016 ± 0.001	0.021 ± 0.009
Fructose	0.050 ± 0.010	0.036 ± 0.008
Glucose	0.058 ± 0.018	0.067 ± 0.020
Myo-inositol	0.366 ± 0.052	0.359 ± 0.053
Trehalose	0.110 ± 0.056	0.223 ± 0.093

The concentration [nmol] of polyols and saccharides detected in 6 × 10^6 cells. Cells were harvested after 72 hours of cultivation in the carbon-rich (rich) and carbon-poor (poor) media, washed in 3.6% sea salt solution and analyzed by GC-MS.

latum was grown in carbon-rich and carbon-poor media and harvested at different time points (24, 72, and 240 hours). The cells were subsequently fixed and labeled with a monoclonal antibody specific for β-1,3-glucan. Cells cultured in the carbon-poor medium stained strongly, particularly after 24 and 72 hours of growth (Fig. 3), whereas the immunofluorescence signal became much weaker in a 10 days-old culture. In cells grown in the carbon-rich medium, the anti-β-1,3-glucan antibody usually recognized just a single cytosolic vesicle of a variable size (Fig. 3). The *E. gracilis* cells, used as a positive control for β-1,3-glucan staining, showed intense fluorescence signal in the complete medium within the first 24 hours of growth, with the intensity of staining decreasing with the cultivation time. *Trypanosoma brucei*, which lacks the capacity to synthesize paramylon and hence does not show any signal with the above antibody, served as a negative control (Fig. 3).

Dynamics of Paramylon Accumulation

Cells were also subjected to the analysis of paramylon accumulation at three time points, namely at 24, 72, and 240 hours after inoculation of the culture (Fig. 1A). For each time point, 3 × 10^7 cells were collected from the carbon-rich and carbon-poor media and subsequently lyophilized. The polysaccharide was then isolated and hydrolyzed to its monomers. We detected paramylon-derived glucose by spectrophotometric measurement only at the 72 hours time point. Glucose concentration was more than four times lower in cells grown in the carbon-rich medium as compared to cells derived from the carbon-poor medium (Fig. 4A).

Trehalose

Under certain cultivation conditions, paramylon degradation in *E. gracilis* is linked with trehalose synthesis (Takenaka et al. 1997). Hence, we focused on this disaccharide, known to be a stress factor. Trehalose was extracted from 3 × 10^7 cells kept for 24, 72, and 240 hours in both the carbon-rich and carbon-poor media. Sugars obtained from the acetone cell fraction were resolved by TLC, where amongst two visualized signals, one co-

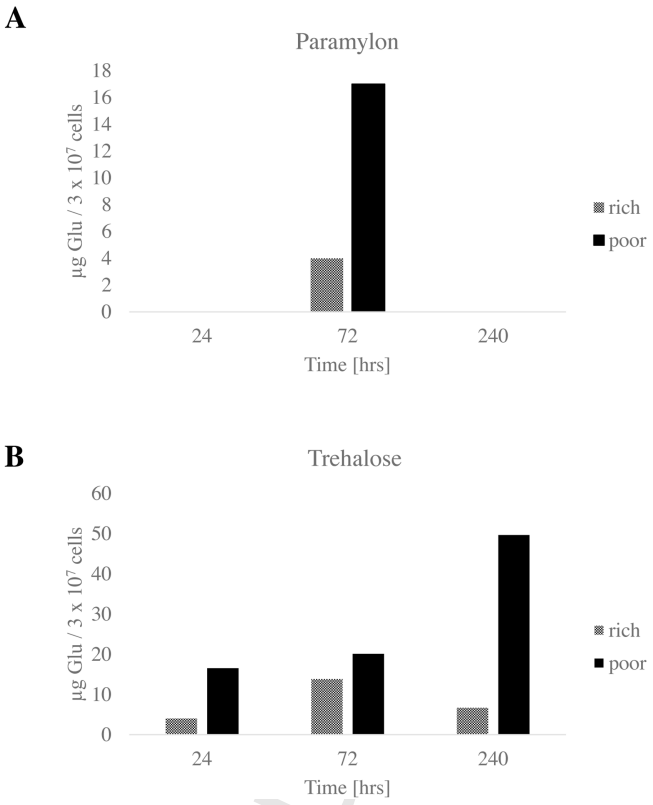

Figure 4. Glucose concentration. Paramylon (**A**) and trehalose (**B**) were isolated and hydrolyzed to their monomers. Glucose concentration was then specified by spectrophotometric measurement. Values of one of three independent experiments are shown. *x* axis – time points of cultivation prior to the sugar extraction; *y* axis – µg of glucose per 3×10^7 cells. Rich – carbon-rich medium; poor – carbon-poor medium.

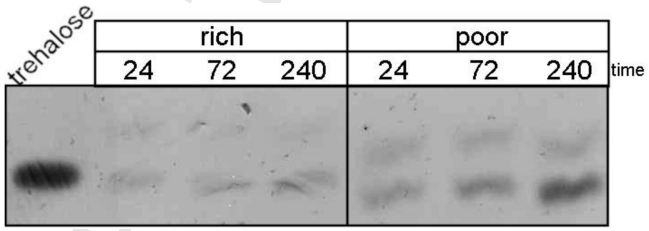

Figure 5. Accumulation of trehalose. After 24, 72 and 240 hours of cultivation in the carbon-rich (rich) or carbon-poor (poor) media, 3×10^7 cells were subjected to the TLC analysis of trehalose.

migrated with the trehalose standard (Fig. 5). Trehalose seemed to be the only variable signal on the TLC profile, as in cells grown in carbon-poor medium, the amount of trehalose increased with time. In contrast, a stably low level of this metabolite was observed in cells grown in the carbon-rich medium (Fig. 5). The same trend was observed at the concentration of glucose obtained by hydrolysis of trehalose isolated from the same cells (Fig. 4B). Through GC–MS analysis, we observed two times higher concentration of trehalose in cells kept for 72 hours in carbon-poor medium, when compared to those in carbon-rich conditions (Table 1).

To determine the origin of glucose forming paramylon and trehalose, cells were fed with radiolabeled ^{14}C-glucose and ^{14}C-proline. When ^{14}C-proline was used, incorporation of the labeled carbon into paramylon and trehalose increased when cells were cultivated in the carbon-poor medium (Tables 2 and 3). When ^{14}C-glucose was used, only a small trace of radiolabeled trehalose was observed in the carbon-poor medium (Table 3).

Table 2. Paramylon labeling with ^{14}C[U] substrates.

^{14}C[U]-	Sample	Radioactivity *dpm*	Total radioactivity taken up *%*
Proline	rich	60	0
	poor	24900	0,3
Glucose	rich	0	0
	poor	0	0

5×10^5 cells were cultivated for 24 hours in the carbon-rich (rich) and carbon-poor (poor) media supplemented with ^{14}C-proline or ^{14}C-glucose. Radioactivity in the isolated paramylon was quantified by Liquid Scintilation Counter; dpm – disintegration per minute.

Table 3. Trehalose labeling with ^{14}C[U] substrates.

^{14}C[U]-	Sample	Radioactivity *dpm*	Total radioactivity taken up *%*
Proline	rich	564800	11,3
	poor	1596000	44,9
Glucose	rich	0	0
	poor	25600	0,4

5×10^5 cells were cultivated for 24 hours in the carbon-rich (rich) and carbon-poor (poor) media supplemented with radioactively labeled ^{14}C-proline or ^{14}C-glucose. Radioactivity in the trehalose containing acetone fraction was quantified by Liquid Scintilation Counter; dpm – disintegration per minute.

To clarify whether proline is the actual precursor used for glucose synthesis, labeled monosaccharides obtained from 5×10^5 *D. papillatum* cells grown in both types of media were purified, separated on TLC and exposed overnight on an X-ray film. The autoradiogram showed high intensity of glucose labeling in the carbon-poor medium (Fig. 6). Moreover, other signals that did not match the used standards (Fig. 6) were still somewhat higher than those in the carbon-rich medium (Fig. 6). Unidentified signals may represent either monosaccharides or amino acids. Mobility of the labeled proline was evaluated using a set of standards. Despite the fact that galactose and ribose were among the prominent sugar monomers together with glucose (Fig. 2C), no labeling of these sugars was intercepted on autoradiogram after 24 hours of labeling (Fig. 6).

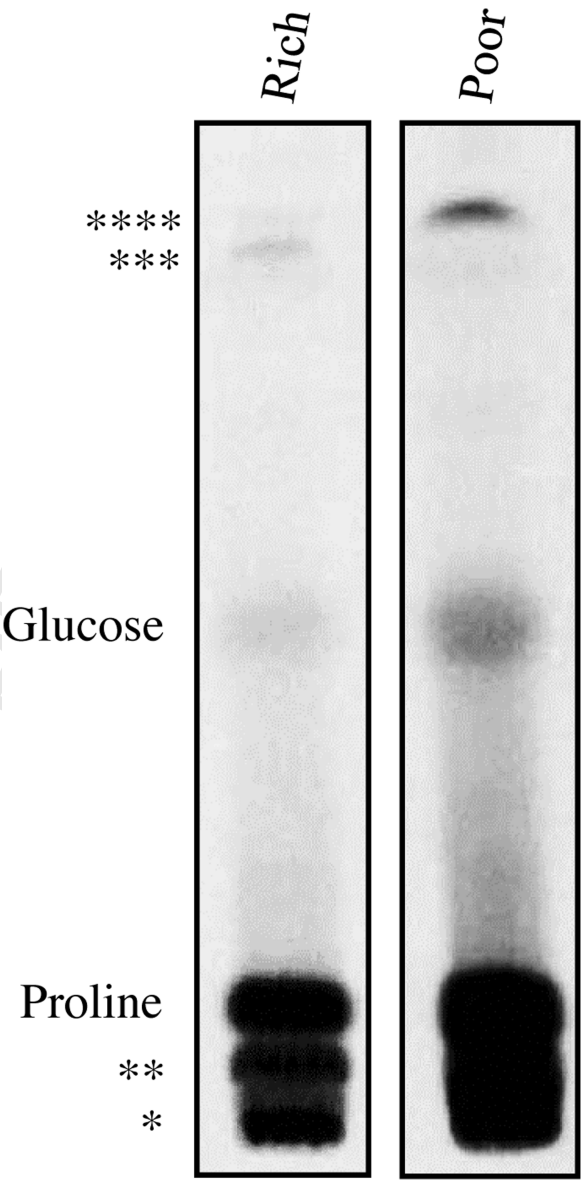

Figure 6. Detection of labeled monosaccharides. Autoradiogram of labeled monosaccharides obtained from 5×10^5 cells grown in the carbon-rich (rich) and carbon-poor media (poor), both supplemented with ^{14}C[U]-proline. Labeled monosaccharides were identified using cold standards. *,** may represent either phosphorylated monosaccharides or amino acids. ***,**** identity of these monosaccharides could not be established using the available standards.

Enzymes of Paramylon Metabolism in Euglenozoans

We have analyzed the sequences of glucan synthase from the genome of *D. papillatum* and

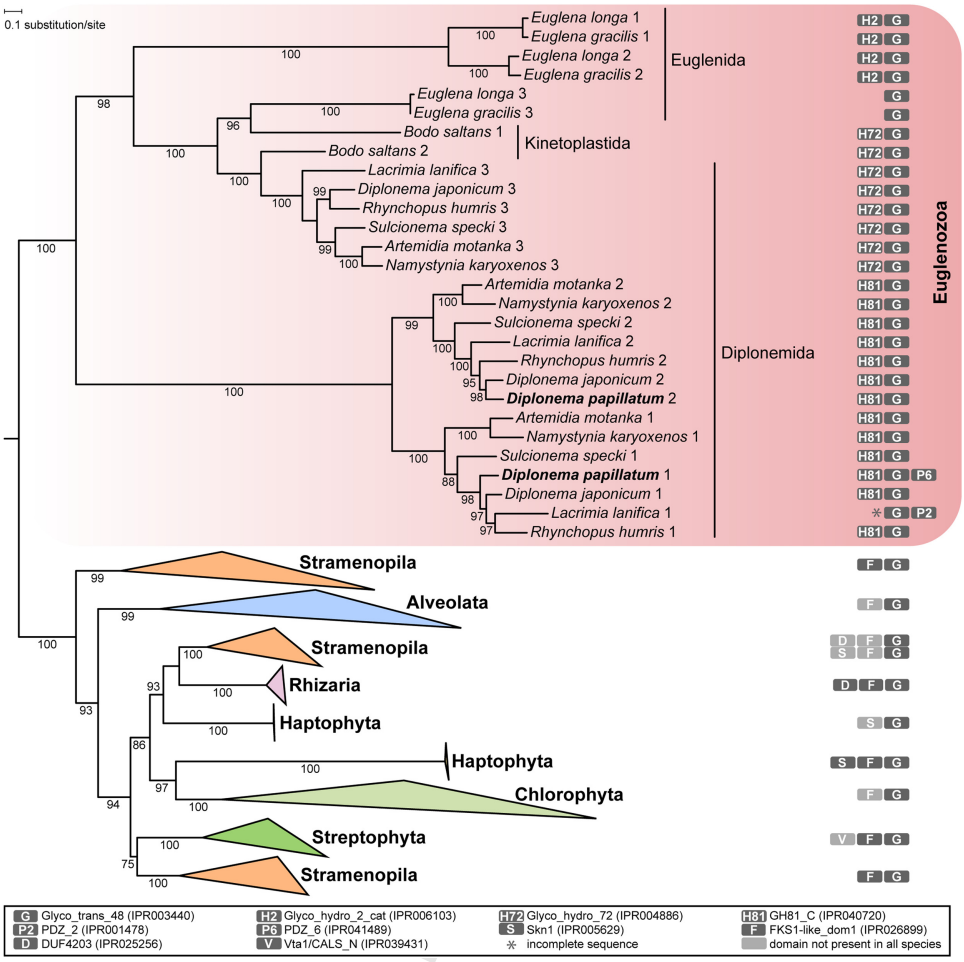

Figure 7. Phylogenetic analysis of glucan synthase proteins. Diplonemid sequences represent two paralogs inside the highly supported euglenozoan clade. For simplicity, broader clades were collapsed and are represented by triangles. Protein domains identified by InterProScan are mapped onto the tree and explained in the graphical legend below the tree. Bootstrap support values are given when $\geq$75. A full version of the tree is provided as Supplementary Material Figure S1.

other diplonemids available in culture (Prokopchuk et al. 2019; Tashyreva et al. 2018a, b). In these genomes, three paralogues of glucan synthase were found, except for *D. papillatum*, which possesses only two of them. Diplonemid sequences form a highly supported monophyletic clade alongside other euglenozoan sequences (*Bodo saltans* representing kinetoplastids, and *Euglena longa* and *E. gracilis* representing euglenids) (Fig. 7; Supplementary Material Fig. S1). Interestingly, the sequences of glucan synthases exhibited an extra domain at their N-termini (Fig. 7). One diplonemid paralog contains an extra glucanosyltransferase domain (GH72, IPR004886; lacking in *D. papillatum*), while the other two paralogs each bear a glycosyl hydrolase domain (GH81, IPR040720) homologous to the glucanases, which may serve in the hydrolysis of paramylon.

A search for glucanases in diplonemids revealed only glucanase domains fused to glucan synthases. No other glucanase sequences were retrieved from the diplonemid dataset, except for *Diplonema japonicum*, which possesses a glucanase without any additional domain, and is unrelated to those synthases with fused architecture yet shows similarity to a sequence retrieved from *B. saltans* (Supplementary Material Fig. S2). Although the posterior mean site frequency method was employed to build the phylogenetic tree (Wang et al. 2018), which should prevent the long-branch attraction phenomenon, we cannot rule out that the clustering of these two sequences may represent

an artifact. Surprisingly, we observed an expansion of the glucanase protein family in euglenids, as they encode 12 paralogs of this enzyme. Two paralogs form a monophyletic group with diplonemids, while the other paralogs are related to stramenopiles (Supplementary Material Fig. S2).

E. gracilis encodes also β-1,3-glucan phosphorylase, another enzyme for paramylon degradation (Kuhaudomlarp et al. 2018). We failed to identify this enzyme in *B. saltans* genome and all of the diplonemid datasets even when HMMER, a more sensitive method than BLAST, was employed. Thus, β-1,3-glucan phosphorylase was apparently acquired in the Euglenid lineage, and the retrieved glucanases are the only enzymes involved in paramylon degradation in diplonemids.

Discussion

Although the synthesis of storage polysaccharide(s) is a highly beneficial metabolic adaptation, it is not as frequent as one would intuitively expect. Indeed, within the widespread and ecologically highly relevant euglenozoan protists, only euglenids are known to be capable of the anabolic pathway of paramylon synthesis. Paramylon is the simplest β-1,3-glucan, insoluble in water, with a linear unbranched structure (Gottlieb 1850). The side-branching changes the physical properties of the polymer from water-insoluble to water-soluble (Westerlund et al. 1993) and hence, not all crystalline glucose polymers may be labeled as paramylon-like structures (Kiss and Triemer 1988). Here we show that a protocol for the isolation of paramylon from *E. gracilis* applied to *D. papillatum* yielded a polymer with identical properties. It is insoluble in water and responsive to acid hydrolysis, which produces glucose monomers. Importantly, *D. papillatum* grown in media with different tryptone content modified the intensity of staining with the antibody against the β-1,3-linkage. This bond connects the glucose monomers, suggesting that the amount of the polymer is subject to significant fluctuations triggered by different concentrations of tryptone, which in itself is a mixture of (non)essential amino acids and longer peptides. This observation links the dynamics of storage to carbon and nitrogen availability.

Paramylon was detected predominantly in cells grown in the carbon-poor medium. Interestingly, this observation is in striking contrast with what has been described for the well-studied *E. gracilis*, where the paramylon synthesis is most active in the first 24 hours of growth in a carbon-rich medium (Briand and Calvayrac 1980). On the contrary, in *D. papillatum* the polysaccharide biogenesis is stimulated by the depletion of carbon and nitrogen in the medium. The dynamics of polymer accumulation is also distinct, with the culmination at 72 hours, followed by a decline. Such dynamics were confirmed by two independent methods, namely by measuring glucose concentration in the isolated polymer, and by immunodetection of the β-1,3-linkage within the cells. To the best of our knowledge, the synthesis of storage macromolecules was documented solely under the nutrient-rich conditions (Barsanti et al. 2001; Pagni et al. 1992; van Loosdrecht et al. 1997), making *D. papillatum* unique in this respect.

Hence, we can only speculate what advantage *D. papillatum* gains from the accumulation of paramylon under carbon-poor conditions. The possibility of a stress response to a shift from glucose-rich conditions to the poor ones can be excluded since the cells used in this study were priorly adapted to long-term cultivation in carbon-poor medium. Moreover, cultivation in different media was accompanied by pronounced changes in cell motility. The lack of nutrients induced the formation of an extremely motile form apparently adapted to active swimming, most probably in order to move into more favorable conditions. Another notable feature restricted to the starving cells was the formation of vacuolar structures in their cytoplasm. Diatoms, another prominent group of marine protists, use extensive formation of vacuoles as a tool for maintaining nutrition and energetic balance under limited resources (Raven 1997). However, in *D. papillatum* the accumulation of paramylon is not in direct correlation with the cytoplasmic vacuolization in the carbon-poor media, since vacuoles remained abundant throughout the 10 days-long period of observation, whereas the amount of paramylon dropped.

It has been previously shown that the uptake of glucose by *D. papillatum* is negligible in carbon-rich medium (Morales et al. 2016). Similar results were also obtained in our experiments, where radiolabeled glucose failed to be incorporated into the isolated paramylon. Feeding *D. papillatum* with ^{14}C-glucose resulted in trace labeling of trehalose under carbon-poor condition, while no labeling was detected in the isolated polymer. ^{14}C-proline was abundantly incorporated into trehalose and to a much smaller extent into paramylon. Therefore, it seems unlikely that *D. papillatum* synthesizes paramylon directly from glucose. Our results indicate that trehalose is synthesized independently of paramylon degradation. This situation is different from what is known for *E. gracilis*, where the

radioactivity of ^{14}C-paramylon was stoichiometrically incorporated into trehalose (Takenaka et al. 1997). This observation is in line with previous findings, according to which the gluconeogenic flux is achieved *via* the metabolism of amino acids associated with re-routing of carbons through the glucan synthase activity, eventually leading to the formation of a carbohydrate polymer (Morales et al. 2016).

Expectedly, in phylogenetic analysis glucan synthases of diplonemids, kinetoplastids and euglenids form a monophyletic clade rather distinct from other eukaryotes. However, a striking difference between the glucan synthases of the marine *D. papillatum* and freshwater *E. gracilis* exists, as the former exhibit an extra N-terminal domain homologous to glucanases. A similar branching order of diplonemid sequences in both glucan synthase and glucanase phylogenies suggests that a fusion of these two domains in the common ancestor of diplonemids was followed by a duplication event. Hence, these two paralogs bear both synthetic and degrading activities.

So far, the carbohydrate metabolism in *D. papillatum* studied under the carbon-rich conditions seemed to lack hexokinase and phosphofructokinase, key enzymes in the phosphorylation of glucose (Morales et al. 2016). This situation was interpreted as leading to a gluconeogenic flux that is further channeled into the pentose phosphate pathway, making use of the synthesized glucose. Our experiments support this view. The most plausible scenario postulates an alternative route using amino acids as gluconeogenic substrate, the product of which is stored in the form of a polysaccharide that maintains viability when the cells are depleted of a constant carbon supply. Such interpretation of the available data implies the existence of several intriguing features: (1) a quorum-sensing system that allows maximum cell growth using gluconeogenesis under the carbon-rich conditions; (2) a secondary system for the re-routing of the gluconeogenic flux towards the activity of glucan synthase, which leads to the stationary growth phase and paramylon synthesis, and, finally (3) glycolysis activated only under certain conditions, particularly when amino acids are not available and the cells contain stored carbon. An alternative for the third requirement is the usage of glucose for the synthesis of trehalose, a non-reducing disaccharide found in most eukaryotes except mammals (Avonce et al. 2006). We suggest that in the carbon-poor medium, trehalose functions as a protectant against protein degradation.

While the carbohydrate synthesis is usually a consequence of an abundant food supply, *D. papillatum* seems to initiate this pathway under low nutrition conditions. Here we propose that paramylon, in which glucose monomers are linked via the β-1,3-glycosidic bond, provides a hitherto unknown function, which may represent one of the key adaptations that are behind the enormous success of the enigmatic diplonemid flagellates in the world's oceans.

Concluding Remarks

Diplonemids successfully inhabit the various depths of the world oceans. Their life strategy is still unknown although several scenarios have been proposed, each of which may be valid under certain conditions. The ability of *D. papillatum*, a model species of the group, to synthesize storage polysaccharides under nutrient-low conditions may point at the phenomenon of a unique metabolic adaptation that allows diplonemids to occupy virtually every niche in the world's oceans including the least habitable zones.

Methods

Cell cultivation: *D. papillatum* cells were inoculated into carbon-rich and carbon-poor media, at a concentration of 5×10^5 cells/ml. The carbon-rich medium contained 36 g/l sea salts, 1 g/l tryptone and 1% (v/v) horse serum, while the carbon-poor medium consisted of 36 g/l sea salts, 0.01 g/l tryptone and 1% (v/v) horse serum. Cells were subjected to long-term cultivation in these media types at 15 °C stationary, with subculturing every seven days. Both cultures were kept in this manner for at least 18 days prior to the experiments, and the growth was monitored on a daily basis. For polymer and sugars isolation, cells were harvested on the third day. For the study of the dynamics of polymer accumulation, cells were collected at three selected time points (24, 72 and 240 hours).

E. gracilis cells were cultivated axenically in Hutner liquid medium (Hutner et al. 1966) at 27 °C under permanent light conditions (10 μm/m^2 s^1) and constant shaking. The procyclic stage of *T. brucei* (strain 29-13) was cultured at 27 °C in SDM79 medium containing 10% (v/v) heat-inactivated fetal bovine serum and 2.5 mg/ml hemin (Changmai et al. 2013).

Light microscopy: For light microscopy imaging, a drop with live cells at three time points

(24, 72 and 240 hours of cultivation) was trapped between a glass slide and a coverslip and examined at 100× under the Olympus BX53 microscope equipped with differential interference contrast (DIC). Recordings were taken with a DP72 digital camera at 1600 × 1200-pixel resolution using CellSens software v. 1.11 (Olympus). The images were processed using Image J v. 1.51 software.

Polysaccharide isolation: For polysaccharide extractions, 4×10^7 cells were harvested from 72 hours-old cultures grown in carbon-rich and carbon-poor media. Cells were collected by centrifugation at 1000 *g* for 10 min, washed in 3.6% sea salts and freeze-dried (Alpha 1-2 LDplus Freeze Dryer). Polymer was extracted as described elsewhere (Tanaka et al. 2017). Briefly, the dried cells were defatted by dual sonication in acetone and samples were spun at 5000 *g* for 5 min. Acetone was retained for further analysis. To remove proteins from the defatted cells, these were resuspended in 1% (w/v) SDS and boiled for 30 min in a water-bath. The polymer was collected by centrifugation at 5000 *g* for 5 min and rinsed once with 0.1% (w/v) SDS and twice with distilled water, undergoing centrifugation under the same conditions between these steps.

Determination of polysaccharide composition: Isolated polysaccharide was hydrolyzed with 500 μl of 2 M trifluoroacetic acid for 2 hours at 120 °C to release monomers. After cooling down to room temperature, samples were dried under nitrogen gas (N_2). Residual trifluoroacetic acid was removed from pellets by two subsequent washes with methanol and distilled water and dried under N_2 between washes. Saccharide monomers were extracted with 1 ml of chloroform:water (1:1). The water phase was evaporated using a vacuum concentrator (CentriVap) and the obtained monosaccharides were dissolved in water and analyzed by thin layer chromatography (TLC) (Kieselgel 60, Merck). Samples were developed twice in ethyl acetate:pyridine:acetic acid:water (6:3:1:1). Standards of 200 nmol, each of rhamnose, ribose, arabinose, mannose, glucose, and galactose were run in the same fashion and visualized by α-naphthol with subsequent heating at 120 °C for 10 min. This process was repeated three times on independent samples.

Total sugars and trehalose extraction: Total monosaccharide profiles were obtained from 4×10^7 cells cultivated for 72 hours in both carbon-rich and carbon-poor media, and samples were processed as described above. The hydrolysates were subjected to TLC analysis on silica gel plates (Kieselgel 60, Merck) developed twice in the mixture of ethyl acetate:pyridine:acetic acid:water (6:3:1:1). Saccharides were visualized as described above, while trehalose was extracted from the acetone fraction obtained after acetone sonication (see Polysaccharide isolation). Acetone was dried under N_2 and trehalose was re-extracted from the pellet by a mixture of chloroform:methanol:water (4:2:1). The water phase was dried using a vacuum concentrator and the samples were resuspended in distilled water and developed together with the trehalose standard by TLC in butanol:methanol:water (5:3:2). Visualization was performed as described above. Three independent experiments were performed.

Determination of glucose concentration: Concentration of glucose in 3×10^7 cells at three time points (24, 72 and 240 hours of cultivation) was identified for paramylon and trehalose hydrolyzed in 2 M trifluoroacetic acid by spectrophotometric method for hexoses at 490 nm in sulfuric acid and phenol (Dubois et al. 1956).

Immunofluorescence analysis: Cells were fixed for 30 min with 4% paraformaldehyde in either artificial sea water for *D. papillatum* or PHEM buffer (Schliwa and van Blerkom 1981) for *E. gracilis* and phosphate buffer (PBS) for *T. brucei*, and allowed to adhere onto poly-L-lysine coated glass slides. The bound cells were permeabilized with 100% ice-cold methanol or 0.1% Igepal in case of *E. gracilis* for 20 min at 4 °C, washed and incubated in the blocking solution (5% nonfat milk, 0.05% Tween-20 in PBS or PHEM containing 3% BSA) for 45 min. The slides were then incubated overnight with monoclonal mouse anti-β-1,3-glucan antibodies (Biosupplies) at a dilution of 1:500, washed with PBS and incubated for 1 hour at room temperature with goat anti-mouse secondary antibody conjugated to Alexa Fluor 555, diluted 1:1000. The samples were subsequently mounted in ProLong Gold antifade reagent (Life Technology) containing 4′,6-diamidino-2-phenylindole (DAPI) and examined by Olympus BX53 fluorescence microscope.

Gas chromatography–mass spectrometry (GC–MS**):** For GC-MS analysis, 6×10^6 cells were collected from carbon-rich and carbon-poor media on the third day after inoculation. Pellets were washed with a salts solution mimicking seawater (450 mM NaCl; 10 mM KCl; 9 mM $CaCl_2$; 30 mM $MgC_{12} \times 6H_2O$; 16 mM $MgSO_4 \times 7H_2O$), collected in an 1.5 ml tube and immediately extracted with 100 μl cold methanol:acetonitrile:water (2:2:1) containing methyl-α-D-glucopyranoside (0.5 ng/μl) as an internal standard. The content was homogenized in an ultrasonic bath at 50 Hz for 5 min and kept at −18 °C. The mixture was centrifuged at

4490 *g* at 4 °C for 5 min and the supernatant was transferred into another vial. The extraction step was repeated with 20 µl of the same extraction medium and the supernatants were combined and evaporated by a vacuum concentrator (Jouan RC 10.10 and RCT 60).

The sample preparation and GC–MS analysis was conducted as described elsewhere (Koštál et al. 2007). Briefly, keto and enol functional groups were oximated with 25 µl *O*-methylhydroxylamine (20 mg/ml pyridine) in 30 µl dimethylformamide at 80 °C for 30 min, and hydroxyls were silylated with 30 µl trimethylsilylimidazol in 70 µl dimethylformamide at 80 °C for 30 min. After re-extraction into 100 µl isooctane, 1 µl aliquot was injected into a DSQ GC–MS single quadrupole mass spectrometer (Thermo Fisher). A 30 m × 0.25 mm × 0.25 mm DB – 1MS capillary column Agilent was used for separation of the metabolites. The instrument settings were: helium flow-rate 1.1 ml/min; inlet temperature, 250 °C; injection mode, splitless; split flow, 20 ml/min; splitless time, 1.3 min; temperature program, 80 °C hold 1 min, 20 °C/min to 180 °C, 5 °C/min to 200 °C, 25 °C/min to 300 °C hold for 3 min; transfer-line temperature 280 °C and electron-ion source temperature, 220 °C, ionization energy 70 eV.

Labeling with ^{14}C[U]-proline or ^{14}C[U]-glucose: Five × 10^5 cells were inoculated into 1 ml of carbon-rich and carbon-poor media on a 24-well plate. Each medium was supplemented with ^{14}C[U]-proline or ^{14}C[U]-glucose at a final concentration 1 µCi/ml and the cells were cultivated for 24 hours at a stationary phase. Cells were collected at 1000 *g* for 10 min, followed with two washes in 36 g/l sea salt solution. The pellets underwent acetone sonication. Next, the pellets and acetone supernatants were processed following the polysaccharide and trehalose extractions described above. Both polysaccharide and trehalose were resuspended in 100 µl of distilled water. Radioactive material was subjected to liquid scintillation spectrometry (Perkin Elmer), quantified as disintegrations per min (dpm) and evaluated in percentage where the amount of dpm in cell culture was taken as 100%. Each experiment was performed in triplicate.

D. papillatum cultures at a concentration of 5 × 10^5 cells/ml were inoculated into 3 ml of carbon-rich and carbon-poor media supplemented with ^{14}C[U]-proline at a final concentration of 1 µCi/ml. Both cultures were kept at stationary phase for 24 hours and the labeled cells were then collected by centrifugation at 1000 *g* for 10 min, followed by two sea salts washes and acetone sonication as described above. In order to identify radiolabeled sugars, the samples were hydrolyzed in 2 M trifluoroacetic acid at 120 °C for 2 hours, dried under N_2, washed twice with methanol, and partitioned between hexane and distilled water. Subsequently, hexane was removed and discarded, and the aqueous phase was dried in a vacuum evaporator (CentriVap). Repeated washes of the hydrolyzed samples with deionized water removed the residual trifluoroacetic acid. The hydrolysates were subjected to the TLC analysis on silica gel plates developed twice in ethyl acetate:pyridine:acetic acid:water (6:3:1:1). Radioactivity was visualized by the exposure of the TLC plates to Kodak X-Omat AR film at −70 °C. Unlabeled standards were visualized by α-naphthol as described above.

Sequence searches and phylogenetic analyses: Glucan synthase sequences were retrieved from NCBI and CryptoDB based on a previous study (Huang et al. 2018). Sequences from *E. gracilis* were reported previously (Tanaka et al. 2017). Sequences from *E. longa* and *D. papillatum* were found by tBLASTn searches in the recently published transcriptomic data (Záhonová et al. 2018) and in an unpublished genome assembly, respectively, using *E. gracilis* sequences as queries. *D. papillatum* sequences served as queries for searches in the transcriptomic data of other diplonemid species, namely *Diplonema japonicum*, *Rhynchopus humris*, *Lacrimia lanifica*, *Sulcionema specki*, *Artemidia motanka*, and *Namystynia karyoxenos*. Sequences from all organisms were submitted to InterProScan and identified protein domains were mapped onto the phylogenetic tree.

Glucanase sequences were retrieved by BLAST searches at NCBI. Identified glucanase domains in diplonemids were used as queries for searches in their transcriptomes. Glucanases from *E. gracilis* reported previously (Novák Vanclová et al. 2020) were used as queries for searches in the *E. gracilis* and *E. longa* transcriptomes.

β-1,3-Glucan phosphorylase was searched in all diplonemid data using *E. gracilis* sequence identified previously (Kuhaudomlarp et al. 2018). Since no homolog was retrieved in any other euglenozoan dataset, a more sensitive method based on profile hidden Markov models, HMMER (Eddy 2009), was employed. To build an HMM profile, all β-1,3-glucan phosphorylase sequences available in the CAZy database (Lombard et al. 2014) were aligned by MAFFT tool (Katoh and Standley 2013).

Since glucan synthase sequences also bear additional domains, these were manually trimmed and only glucan synthase domains were aligned. In case of diplonemid glucanases, glucan syn-

thase domains were trimmed and only glucanase domains were aligned with glucanase proteins from other organisms. Both alignments were produced by the MAFFT tool and are available upon request from the corresponding author. To remove poorly aligned positions, the trimAL tool was used (Capella-Gutiérrez et al. 2009). Maximum likelihood trees were inferred from the alignments using the LG + C20+F + G model and the posterior mean site frequency method (Wang et al. 2018) in the IQ-TREE software (Nguyen et al. 2015) and employing the strategy of rapid bootstrapping followed by a "thorough" maximum likelihood search with 1000 bootstrap replicates.

Conflict of Interest

The authors declare no conflict of interest.

Acknowledgements

We highly appreciate access to the genome assembly of *D. papillatum* kindly provided by Gertraud Burger (University of Montreal). We acknowledge computation resources provided by CERIT-SC and MetaCentrum Brno. This work was supported by the Czech Grant Agency grant 18-15962S, ERC CZ LL1601, and the ERD Funds projectOPVVV0000759 (to JL), the Grant Agency of the Slovak Ministry of Education and the Academy of Sciences 1/0387/17, the Slovak Research and Development Agency grant APVV-0286-12 (to AH) and the Grant Agency of the Slovak Ministry of Education and the Academy of Sciences 1/0781/19.

Appendix A. Supplementary Data

Supplementary material related to this article can be found, in the online version, at doi:https://doi.org/10.1016/j.protis.2020.125717.

References

Adl SM, Bass D, Lane Ch E, Lukeš J, Schoch CL, Smirnov A, Agatha S, Berney C, Brown MW, Burki F, Cárdenas P, Čepička I, Chistyakova L, del Campo J, Dunthorn M, Edvardsen B, Eglit Y, Guillou L, Hampl V, Heiss AA, Hoppenrath M, James TY, Karnkowska A, Karpov S, Kim E, Kolisko M, Kudryavtsev A, Lahr DJG, Lara E, Le Gall L, Lynn DH, Mann DG, Massana R, Mitchell EAD, Morrow C, Park JS, Pawlowski JW, Powell MJ, Richter DJ, Rueckert S, Shadwick L, Shimano S, Spiegel FW, Torruella G, Youssef N, Zlatogursky V, Zhang Q (2018) Revisions to the classification, nomenclature, and diversity of eukaryotes. J Eukaryot Microbiol **66**:4–119

Allmann S, Mazet M, Ziebart N, Bouyssou G, Fouillen L, Dupuy JW, Bonneu M, Moreau P, Bringaud F, Boshart M (2014) Triacylglycerol storage in lipid droplets in procyclic *Trypanosoma brucei*. PLoS ONE **9**:e114628

Allmann S, Morand P, Ebikeme C, Gales L, Biran M, Hubert J, Brennand A, Mazet M, Franconi JM, Michels PA, Portais JC, Boshart M, Bringaud (2013) Cytosolic NADPH homeostasis in glucose-starved procyclic *Trypanosoma brucei* relies on malic enzyme and the pentose phosphate pathway fed by gluconeogenic flux. J Biol Chem **288**:18494–18505

Archibald AR, Cunningham WL, Manners DJ, Stark JR, Ryley JF (1963) Metabolism of the protozoa, X. The molecular structure of the reserve polysaccharides from *Ochromonas malhamensis* and *Peranema trichophorum*. Biochem J **88**:444–451

Aspinall GO, Kessler G (1957) The structure of callose from the grape vine. Chem Ind (London) **1296**

Avonce N, Mendoza-Vargas A, Morett E, Iturriaga G (2006) Insights on the evolution of trehalose biosynthesis. BMC Evol Biol **19**:109

Bakker BM, Mensonides FI, Teusink B, van Hoek P, Michels PA, Westerhoff HV (2000) Compartmentation protects trypanosomes from the dangerous design of glycolysis. Proc Natl Acad Sci USA **97**:2087–2092

Barsanti L, Vismara R, Passarelli V, Gualtieri P (2001) Paramylon (β-1,3-glucan) content in wild type and WZSL mutant of *Euglena gracilis*. Effects of growth conditions. J Appl Phycol **13**:59–65

Bäumer D, Preisfeld A, Ruppel HG (2011) Isolation and characterization of paramylon synthase from *Euglena gracilis* (Euglenophyceae). J Phycol **37**:38–46

Blum JJ (1993) Intermediary metabolism of *Leishmania*. Parasitol Today **9**:118–122

Booy FP, Chanzy H, Boudet A (1981) An electron diffraction study of paramylon storage granules from *Euglena gracilis*. J Microsc **12**:133–140

Briand J, Calvayrac R (1980) Paramylon synthesis in heterotrophic and photoheterotrophic *Euglena (*Euglenophyceae). J Phycol **16**:234–239

Bringaud F, Rivière L, Coustou V (2006) Energy metabolism of trypanosomatids: adaptation to available carbon sources. Mol Biochem Parasitol **149**:1–9

Calvayrac R, Laval-Martin D, Briand J, Farineau J (1981) Paramylon synthesis by *Euglena gracilis* photoheterotrophically grown under low O_2 pressure: Description of a mitochloroplast complex. Planta **153**:6–13

Capella-Gutiérrez S, Silla-Martínez JM, Gabaldón T (2009) trimAl: a tool for automated alignment trimming in large-scale phylogenetic analyses. Bioinformatics **25**:1972–1973

Changmai P, Horáková E, Long S, Černotíková-Stříbrná E, McDonald LM, Bontempi EJ, Lukeš J (2013) Both human ferredoxins equally efficiently rescue ferredoxin deficiency in *Trypanosoma brucei*. Mol Microbiol **89**:135–151

Clarke AE, Stone BA (1960) Structure of the paramylon from *Euglena gracilis*. Biochim Biophys Acta **44**:161–163

Coustou V, Besteiro Biran M, Diolez P, Bouchaud V, Voisin P, Michels PA, Canioni P, Baltz T, Bringaud F (2003) ATP generation in the *Trypanosoma brucei* procyclic form: cytosolic substrate level is essential, but not oxidative phosphorylation. J Biol Chem **278**:49625–49635

de Vargas C, Audic S, Henry N, Decelle J, Mahé F, Logares R, Lara E, Berney C, Le Bescot N, Probert I, Carmichael M, Poulain J, Romac S, Colin S, Aury J-M, Bittner L, Chaffron S, Dunthorn M, Engelen S, Flegontova O, Guidi L, Horák A, Jaillon O, Lima-Mendez G, Lukeš J, Malviya S, Morard R, Mulot M, Scalco E, Siano R, Vincent F, Zingone A, Dimier C, Picheral M, Searson S, Kandels-Lewis S, Tara Oceans Coordinators, Acinas SG, Bork P, Bowler C, Gorsky G, Grimsley N, Hingamp P, Iudicon D, Not F, Ogata H, Pesant S, Raes J, Sieracki ME, Speich D, Stemmann L, Sunagawa S, Weissenbach J, Wincker P, Karsenti E (2015) Eukaryotic plankton diversity in the sunlit ocean. Science **348**:1261605

Dubois M, Gilles KA, Hamilton JK, Rebers PA, Smith F (1956) Colorimetric method for determination of sugars and related substances. Anal Chem **28**:350–356

Dwyer MR, Smillie RM (1970) A light-induced beta-1,3-glucan breakdown associated with the differentiation of chloroplasts in *Euglena gracilis*. Biochim Biophys Acta **216**:392–401

Eddy SR (2009) A new generation of homology search tools based on probabilistic inference. Genome Inform **23**:205–211

Flegontova O, Flegontov P, Malviya S, Audic S, Wincker P, de Vargas C, Bowler C, Lukeš J, Horák A (2016) Extreme diversity of diplonemid eukaryotes in the ocean. Curr Biol **26**:3060–3065

Gottlieb J (1850) Ueber eine neue, mit Starkmehl isomere Substanz. Ann Chem Pharm **75**:51–61

Haanstra JR, González-Marcano EB, Gualdrón-López M, Michels PA (2016) Biogenesis, maintenance and dynamics of glycosomes in trypanosomatid parasites. Biochim Biophys Acta **1863**:1038–1048

Harada T, Misaki A, Saito H (1968) Curdlan: a bacterial gel-forming β-D-1,3-glucan. Arch Biochem Biophys **124**:292–298

Henrissat B (1991) A classification of glycosyl hydrolases based on amino acid sequence similarities. Biochem J **280**:309–316

Henrissat B, Bairoch A (1996) Updating the sequence-based classification of glycosyl hydrolases. Biochem J **316**:695–696

Henrissat B, Davies G (1997) Structural and sequence-based classification of glycoside hydrolases. Curr Opin Struct Biol **7**:637–644

Huang W, Haferkamp I, Lepetit B, Molchanova M, Hou S, Jeblick W, Río Bártulos C, Kroth PG (2018) Reduced vacuolar β-1,3-glucan synthesis affects carbohydrate metabolism as well as plastid homeostasis and structure in *Phaeodactylum tricornutum*. Proc Natl Acad Sci USA **115**:4791–4796

Hutner SH, Zahalsky AC, Aaronson S, Baker H, Frank HO (1966) Culture media for *Euglena gracilis*. Meth Cell Biol **2**:217–228

Katoh K, Standley DM (2013) MAFFT multiple sequence alignment software version 7: improvements in performance and usability. Mol Biol Evol **30**:772–780

Kaur B, Valach M, Peña-Diaz P, Moreira S, Keeling PJ, Burger G, Lukeš J, Faktorová D (2018) Transformation of *Diplonema papillatum*, the type species of the highly diverse and abundant marine microeukaryotes Diplonemida (Euglenozoa). Environ Microbiol **20**:1030–1040

Keeling PJ, del Campo J (2017) Marine protists are not just big bacteria. Curr Biol **27**:541–549

Keeling PJ, Burki F, Wilcox HM, Allam B, Allen EE, Amaral-Zettler LA, Armbrust EV, Archibald JM, Bharti AK, Bell CJ, Beszteri B, Bidle KD, Cameron CT, Campbell L, Caron DA, Ann Cattolico RA, Collier JL, Coyne K, Davy SK, Deschamps P, Dyhrman ST, Edvardsen B, Gates RD, Gobler CJ, Greenwood SJ, Guida SM, Jacobi JL, Jakobsen KS, James ER, Jenkins B, John U, Johnson MD, Juhl AR, Kamp A, Katz LA, Kiene R, Kudryavtsev A, Leander BS, Lin S, Lovejoy C, Lynn D, Marchetti A, McManus G, Nedelcu AM, Menden-Deuer S, Miceli C, Mock T, Montresor M, Moran MA, Murray S, Nadathur Nagai S, Ngam PB, Palenik B, Pawlowski J, Petroni G, Piganeau G, Posewitz MC, Rengefors K, Romano G, Rumpho ME, Rynearson T, Schilling KB, Schroeder DC, Simpson AGB, Slamovits CH, Smith DR, Smith GJ, Smith SR, Sosik HM, Stief P, Theriot E, Twary SN, Umale PE, Vaulot D, Wawrik B, Wheeler GL, Wilson WH, Xu Y, Zingone A, Worden AZ (2014) The marine microbial eukaryote transcriptome sequencing project (MMETSP): Illuminating the functional diversity of eukaryotic life in the oceans through transcriptome sequencing. PLoS Biol **12**: e1001889

Kiss JZ, Triemer RE (1988) A comparative study of the storage carbohydrate granules from *Euglena* (Euglenida) and *Pavlova* (Prymnesiida). J Eukaryot Microbiol **35**:237–241

Kondo Y, Kato A, Hojo H, Nozoe S, Takeuchi M, Ochi K (1992) Cytokine-related immunopotentiating activities of paramylon, a beta-(1→3)-D-glucan from *Euglena gracilis*. J Pharmacobiodyn **15**:617–621

Koštál V, Zahradničková H, Šimek P, Zelený J (2007) Multiple component system of sugars and polyols in the overwintering spruce bark beetle, *Ips typographus*. J Insect Physiol **53**:580–586

Kuhaudomlarp S, Patron NJ, Henrissat B, Rejzek M, Saalbach G, Field RA (2018) Identification of *Euglena gracilis* β-1,3-glucan phosphorylase and establishment of a new glycoside hydrolase (GH) family GH149. J Biol Chem **293**:2865–2876

Lara E, Moreira D, Vereshchaka A, Lopez-Garcia P (2009) Panoceanic distribution of new highly diverse clades of deep-sea diplonemids. Environ Microbiol **11**:47–55

Lombard V, Golaconda Ramulu H, Drula E, Coutinho PM, Henrissat B (2014) The carbohydrate-active enzymes database (CAZy) in 2013. Nucleic Acids Res **42(D1)**:D490–D495

Marechal LR, Goldemberg SH (1964) Uridine diphosphate glucose-beta-1,3-glucan beta-3-glucosyltransferase from *Euglena gracilis*. J Biol Chem **239**:3163–3167

Millerioux Y, Ebikeme C, Biran M, Morand P, Bouyssou G, Vincent IM, Mazet M, Riviere L, Franconi JM, Burchmore RJ, Moreau P, Barrett MP, Bringaud F (2013) The threonine degradation pathway of the *Trypanosoma brucei* procyclic form: the main carbon source for lipid biosynthesis is under metabolic control. Mol Microbiol **90**:114–129

Monfils AK, Triemer RE, Bellairs EF (2011) Characterization of paramylon morphological diversity in photosynthetic euglenoids (Euglenales, Euglenophyta). Phycologia **50**:156–169

Morales J, Hashimoto M, Williams TA, Hirawake-Mogi H, Makiuchi T, Tsubouchi A, Kaga N, Taka H, Fujimura T, Koike M, Mita T, Bringaud F, Concepción JL, Hashimoto T, Embley TM, Nara T (2016) Differential remodeling of peroxisome function underpins the environmental and metabolic adaptability of diplonemids and kinetoplastids. Proc Biol Sci **283**:20160520

Muchut RJ, Calloni R, Herrera FE, Garay SA, Arias DG, Iglesias AA, Guerrero SA (2018) Elucidating paramylon and other carbohydrate metabolism in *Euglena gracilis*: Kinetic characterization, structure and cellular localization of UDP-glucose pyrophosphorylase. Biochimie **154**:176–186

Nakashima A, Sugimoto R, Suzuki K, Shirakata Y, Hashiguchi T, Ch Yoshida, Nakano Y (2019) Anti-fibrotic activity of *Euglena gracilis* and paramylon in a mouse model of non-alcoholic steatohepatitis. Food Sci Nutr **7**:139–147

Nguyen LT, Schmidt HA, von Haeseler A, Minh BQ (2015) IQ-TREE: a fast and effective stochastic algorithm for estimating maximum-likelihood phylogenies. Mol Biol Evol **32**:268–274

Novák Vanclová AMG, Zoltner M, Kelly S, Soukal P, Záhonová K, Füssy Z, Ebenezer E, Lacová Dobáková E, Eliáš M, Lukeš J, Field MC, Hampl V (2020) Metabolic quirks and the colourful history of the *Euglena gracilis* secondary plastid. New Phytol **225**:1578–1592

Okouchi R, E S, Yamamoto K, Ota T, Seki K, Imai M, Ota R, Asayama Y, Nakashima A, Suzuki K, Tsuduki T (2019) Simultaneous intake of *Euglena gracilis* and vegetables exerts synergistic anti-obesity and anti-inflammatory effects by modulating the gut microbiota in diet-induced obese mice. Nutrients **11**:E204

Opperdoes FR, Borst P (1977) Localization of nine glycolytic enzymes in a microbody-like organelle in *Trypanosoma brucei*: the glycosome. FEBS Lett **80**:360–364

Pagni M, Beffa T, Isch C, Aragno M (1992) Linear growth and poly(beta-hydroxybutyrate) synthesis in response to pulse-wise addition of the growth-limiting substrate to steady-state heterotrophic continuous cultures of *Aquaspirillum autotrophicum*. J Gen Microbiol **138**:429–436

Prokopchuk G, Tashyreva D, Yabuki A, Horák A, Masařová P, Lukeš J (2019) Morphological, ultrastructural, motility and evolutionary characterization of two new Hemistasiidae species. Protist **170**:259–282

Ralton JE, Naderer T, Piraino HL, Bashtannyk TA, Callaghan JM, McConville MJ (2003) Evidence that intracellular beta1-2 mannan is a virulence factor in *Leishmania* parasites. J Biol Chem **278**:40757–40763

Raven JA (1997) The vacuole: a cost benefit analysis. Adv Bot Res **35**:59–86

Schliwa M, van Blerkom J (1981) Structural interaction of cytoskeletal components. J Cell Biol **90**:222–235

Schwartzbach SD, Schiff JA, Goldstein NH (1975) Events surrounding the early development of *Euglena* chloroplasts. Plant Physiol **56**:313–317

Sernee MF, Ralton JE, Dinev Z, Khairallah GN, O'Hair RA, Williams SJ, McConville MJ (2006) *Leishmania* beta-1,2-mannan is assembled on a mannose-cyclic phosphate primer. Proc Natl Acad Sci USA **103**:9458–9463

Smith TK, Bringaud F, Nolan DP, Figueiredo LM (2017) Metabolic reprogramming during the *Trypanosoma brucei* life cycle. F1000Res **6**:683

Sugimoto R, Ishibashi-Ohgo N, Atsuji K, Miwa Y, Iwata O, Nakashima A, Suzuki K (2018) Euglena extract suppresses adipocyte-differentiation in human adipose-derived stem cells. PLoS ONE **13**:e0192404

Szöor B, Haanstra JR, Gualdrón-López M, Michels PA (2014) Evolution, dynamics and specialized functions of glycosomes in metabolism and development of trypanosomatids. Curr Opin Microbiol **22**:79–87

Takenaka S, Kondo T, Nazeri S, Tamura Y, Tokunaga M, Tsuyama S, Miyatake K, Nakano Y (1997) Accumulation of trehalose as a compatible solute under osmotic stress in *Euglena gracilis* Z. J Eukaryot Microbiol **44**:609–613

Tanaka Y, Ogawa T, Maruta T, Yoshida Y, Arakawa K, Ishikawa T (2017) Glucan synthase-like 2 is indispensable for paramylon synthesis in *Euglena gracilis*. FEBS Lett **591**:1360–1370

Tashyreva D, Prokopchuk G, Votýpka J, Yabuki A, Horák A, Lukeš J (2018a) Life cycle, ultrastructure, and phylogeny of new diplonemids and their endosymbiotic bacteria. mBio **9**:e02447–17

Tashyreva D, Prokopchuk G, Yabuki A, Kaur B, Faktorová D, Votýpka J, Kusaka C, Fujikura K, Shiratori T, Ishida KI, Horák A, Lukeš J (2018b) Phylogeny and morphology of new diplonemids from Japan. Protist **169**:158–179

Valach M, Moreira S, Hoffmann S, Stadler PF, Burger G (2017) Keeping it complicated: Mitochondrial genome plasticity across diplonemids. Sci Rep **7**:14166

van Loosdrecht MCM, Pot MA, Heijnen JJ (1997) Importance of bacterial storage polymers in bioprocceses. Water Sci Tech **35**:41–47

Wang HC, Minh BQ, Susko E, Roger AJ (2018) Modeling site heterogeneity with posterior mean site frequency profiles accelerates accurate phylogenomic estimation. Syst Biol **67**:216–235

Warsi SA, Whelan WJ (1957) Structure of pachyman, the polysaccharide component of *Poria cocos*. Chem Ind (London) **1573**

Watanabe T, Shimada R, Matsuyama A, Yuasa M, Sawamura H, Yoshida E, Suzuki K (2013) Antitumor activity of the β-glucan paramylon from *Euglena* against preneoplastic colonic aberrant crypt foci in mice. Food Funct **4**:1685–1690

Westerlund E, Andersson R, Åman P (1993) Isolation and chemical characterization of water soluble mixed-linked beta-

glucans and arabinoxylans in oat milling fractions. Carbohydr Polym **20**:115–123

Worden AZ, Follows MJ, Giovannoni SJ, Wilken S, Zimmerman AE, Keeling PJ (2015) Environmental science. Rethinking the marine carbon cycle: factoring in the multifarious lifestyles of microbes. Science **347**:1257594

Záhonová K, Füssy Z, Birčák E, Novák Vanclová AMG, Klimeš V, Vesteg M, Krajčovič J, Oborník M, Eliáš M (2018) Peculiar features of the plastids of the colourless alga *Euglena longa* and photosynthetic euglenophytes unveiled by transcriptome analyses. Sci Rep **8**:17012